

## Testing limits of statistical hadronization

Johann Rafelski<sup>a\*</sup> and Jean Letessier<sup>b†</sup>

<sup>a</sup>Department of Physics, University of Arizona, Tucson, AZ 85721

<sup>b</sup>Laboratoire de Physique Théorique et Hautes Energies  
Université Paris 7, 2 place Jussieu, F-75251 Cedex 05.

Much of the energy of the nuclei colliding at RHIC or SPS is converted into final state hadronic particles. About a quarter of this energy is in baryons and antibaryons. There are nearly 10 strange quark pairs per central rapidity participant. Do we really understand the hadronic particle yields? Do we need to introduce post-Fermi-model ideas such as chemical non-equilibrium in order to understand how a deconfined state hadronizes?

### 1. STATISTICAL HADRONIZATION

Statistical Fermi-Pomeranchuk models have been used extensively to study particle yields and spectra since 1950 [1,2]. This approach was developed as a qualitative description of the gross features of particle production. It was originally not meant to be theoretically an accurate picture, just a phase space estimate of what Fermi called an upper limit on particle production in strong interaction processes. In fact, Fermi defined the limitations of the statistical approach stating three conditions: 1) exclusion of particles such as photons which have weak coupling to the interacting system; 2) absence of absolute chemical (abundance) equilibrium for many semi-weakly coupled particles; 3) requirement of relative baryochemical equilibrium. At that time strangeness was not yet discovered, and today we can add 3b) requirement of relative strangeness equilibrium.

In the ensuing decade, another important feature of the strong interactions was discovered: the existence of numerous hadronic resonances. This property of hadronic interactions poses a challenge for the statistical hadronization model as the yield of particles is sensitive to the unidentified high mass hadron resonance states. We will discuss how this influences the expected particle yields in section 2. Our objective is to establish the magnitude of systematic theoretical error we have to expect given incomplete knowledge of the hadronic mass spectrum. A tacit assumption in our approach is that hadron-hadron interaction is well described by the formation of resonant states, and the remaining residual forces are negligible in comparison to the available energy content per particle.

Understanding the hadro-chemistry, *i.e.*, of the composition of particles produced, can finger-print the phase of matter which has undergone statistical hadronization. Therefore, we will describe how chemical parameters, the chemical potentials  $\mu_i$  and the phase space

---

\*Supported by grant DE-FG03-95ER40937 from the U.S. Department of Energy.

†LPTHE, Univ. Paris 6 et 7 is: Unité mixte de Recherche du CNRS, UMR7589.

occupancy parameters  $\gamma_i$ , allow to regulate the particle number. We show how the chemical non-equilibrium is characterized in section 3. We then demonstrate, in section 4, that the *nearly complete particle production results* force upon us the study of chemical non-equilibrium. We demonstrate in particular that a precise description of all RHIC results obtained at  $\sqrt{s_{\text{NN}}} = 130$  GeV (RHIC-130) is possible within the scheme we propose.

## 2. EXPONENTIAL HADRON MASS SPECTRUM

Fermi's statistical model provided the intellectual environment for the theoretical understanding of the exponentially growing hadronic mass spectrum within the statistical bootstrap model invented by Rolf Hagedorn [3]. Hagedorn recognized early on that the large number of different hadronic states, and the increase in their number with their mass, has great practical implications for the behavior of matter at high temperature, and can lead to the formation of a new phase of matter.

Within Fermi's statistical model the number of heavy hadron resonances produced is exponentially suppressed with the ratio of the mass of the particle considered to the temperature present. In spite of this, if the number of different resonances per unit of mass, the mass spectrum  $\rho(m)$ , increases exponentially,

$$\rho(m) \propto (m_0^2 + m^2)^{a/2} e^{\frac{m}{T_H}}, \quad (1)$$

there still would be a critical temperature of hadronic matter, corresponding to the (inverse) slope  $T_H$  of the exponential mass spectrum:

$$\ln \mathcal{Z} = \int d^3x \int \frac{d^3p}{(2\pi)^3} \int dm e^{-\frac{\sqrt{m^2+p^2}}{T}} \rho(m) \bigg|_{T \rightarrow T_H} \rightarrow \infty, \quad \text{for } a > -\frac{5}{2}. \quad (2)$$

Hagedorn called this the boiling of hadronic matter [4]. Hot hadronic matter behaved at this point in the same way as in high temperature 1st order phase transition [5,6].

There is strong empirical evidence that the experimental mass spectrum grows exponentially at least in the interval of interest to the study of particle production [7,8]. Smoothed mass spectrum based on 4627 states known in 1996 is shown as a short dashed line in figure 1, while the 1411 states of 1966, used by Hagedorn [9], are depicted by long dashed line in figure 1. The solid line is a fit to the experimental mass spectrum Eq. (1) with the assumed value  $a = -3$  which yields  $T_H = 158$  MeV.

Proposing that the solid line describes reasonably the mass spectrum, we see that a significant number of resonances remains to be identified for  $m > 1.4$  GeV (note the logarithmic scale in the figure 1). When a study of particle yields is made, a significant systematic uncertainty derived from the lack of knowledge of hadronic mass spectrum can arise, in particular so for models finding relatively high statistical hadronization temperatures. At a hadronization temperature of  $T_h = 145$  MeV, a study of the properties of the particle yields suggests that only about 5% of pions are 'missing'. However, at  $T_h \simeq 175$  MeV [10], this increases to 35%, and the high value of temperature considered poses a practical challenge, since the Statistical Bootstrap model and the Lattice-QCD results for 2+1 flavors [11] are converging to a critical temperature at  $T_H \lesssim 160$  MeV.

One way to assess the magnitude of the systematic error is to compare the properties of the hadron gas using the mass spectrum of the type given in Eq. (1) with that studied

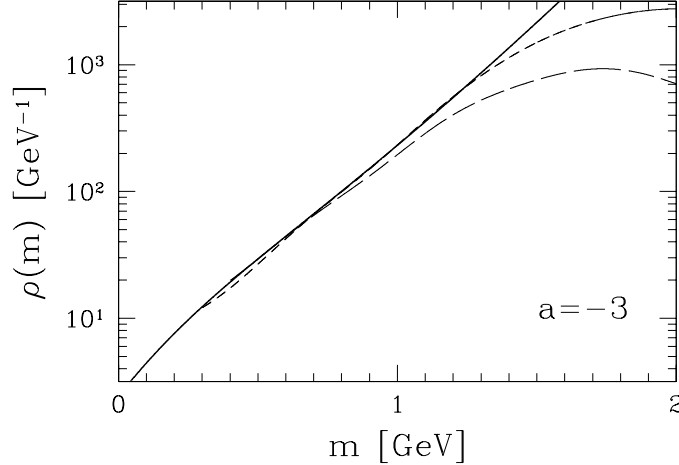


Figure 1. Hadronic mass spectrum: solid line is the best-fit theoretical extrapolation, dashed lines: experimental data (short dashed of 1996, long dashed of 1967).

using the currently known experimental mass spectrum. For a range of values  $a = -2.5$  (most divergent curve in left frame in figure 2) and  $a = -7$ , the energy density  $\varepsilon$  (solid lines) and pressure  $P$  (dashed lines), both scaled with  $T^4$ , are compared to the values obtained summing all known hadronic states (thin line in figure 2). The differences as expected are dramatic at high temperature, near to the boiling point of hadronic matter.

It turns out that the problem is reduced considering the hadron proper volume [5]. Reconsidering the energy density assuming a proper energy density of hadrons as derived from the bag constant  $\mathcal{B} = (190 \text{ MeV})^4$ , we find that the expected excess counting the energy density degrees of freedom remains at the level of 10% as is seen in right frame in figure 2. While this allows to apply statistical hadronization method in study of particle abundance ratios, the influence of quantitatively uncertain finite size correction is very large, implying in particular in the pion yield a considerable systematic theoretical error.

### 3. CHEMICAL NONEQUILIBRIUM

In general the fugacity  $\Upsilon_i$  of each individual particle will comprise the two chemical factors associated with the two different chemical equilibria. For example, let us look at the nucleon, and the antinucleon fugacity and chemical potentials:

$$\Upsilon_N = \gamma_N e^{\mu_B/T}, \quad \Upsilon_{\bar{N}} = \gamma_{\bar{N}} e^{-\mu_B/T}; \quad \sigma_N \equiv \mu_B + T \ln \gamma_N, \quad \sigma_{\bar{N}} \equiv -\mu_B + T \ln \gamma_{\bar{N}}. \quad (3)$$

There is an obvious difference between the two chemical factors in Eq. (3): the number of nucleon-antinucleon pairs is associated with the value of  $\gamma_N$  but not with  $\mu_B$ . This can be seen looking at the first law of thermodynamics, in this context written as:

$$\begin{aligned} dE &= -P dV + T dS + \sigma_N dN + \sigma_{\bar{N}} d\bar{N}, \\ &= -P dV + T dS + \mu_B (dN - d\bar{N}) + T \ln \gamma_N (dN + d\bar{N}). \end{aligned} \quad (4)$$

To obtain the second form, we have employed Eq. (3). We see that  $\mu_B$  is the energy required to change the baryon number,  $B \equiv N - \bar{N}$ , by one unit, while the number of

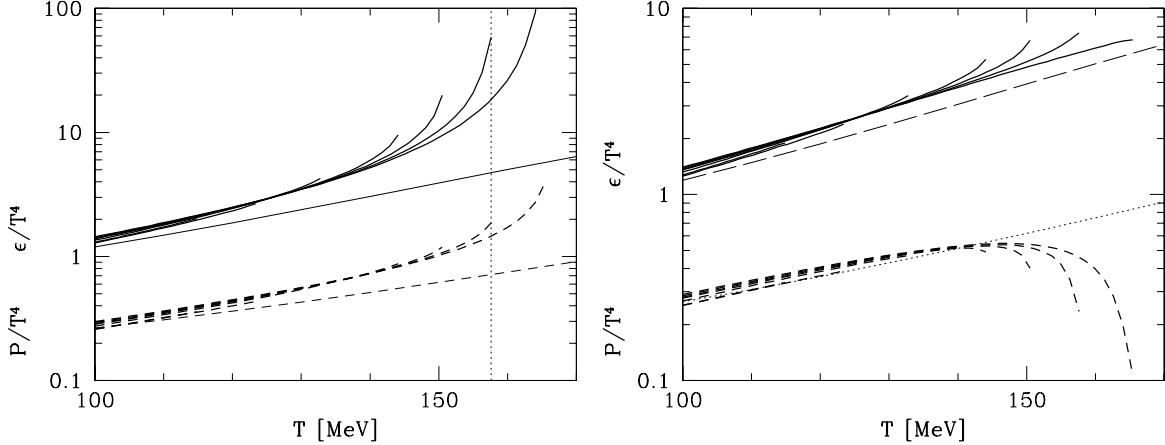


Figure 2. The energy density  $\varepsilon$  (solid lines) and pressure  $P$  (dashed lines), both scaled with  $T^4$ . Left: point hadrons with an exponential mass spectrum (thick lines) are compared to results using known hadrons (thin line). Right: hadron gas with finite volume correction, see text for more detail.

nucleon-antinucleon pairs,  $2N_{\text{pair}} \equiv N + \bar{N}$ , is related to  $\gamma_N$ . For  $\gamma_N \rightarrow 1$ , the last term vanishes, at this point small fluctuation in number of nucleon pairs does not influence the energy of the system, we have reached the absolute baryochemical equilibrium.

It is convenient to follow the quark flavor even in the study of hadron yields, since this allows to keep the same notation across the phase boundary of quark matter and hadronic gas matter. We use:

$$\lambda_u = e^{\mu_u/T}, \quad \lambda_d = e^{\mu_d/T}, \quad \lambda_s = e^{\mu_s/T}, \quad \mu_q = \frac{1}{2}(\mu_u + \mu_d), \quad \lambda_q^2 = \lambda_u \lambda_d. \quad (5)$$

When the light flavors  $u, d$  remain indistinguishable we introduce  $\lambda_q$ .

The relationship of baryochemical potential  $\mu_B$  and of strangeness chemical  $\mu_S$  to quark chemical potential is:

$$\mu_B = 3\mu_q, \quad \lambda_B = \lambda_q^3, \quad \lambda_S = \frac{\lambda_q}{\lambda_s}, \quad \mu_S = \frac{1}{3}\mu_B - \mu_s. \quad (6)$$

These relations arise considering that three quarks make a baryon, and remembering that strange quarks carry *negative* strangeness and one third of baryon number.

When using of fugacities which follow the valance quarks,  $\lambda_i$ ,  $i = u, d, s$ , hadronic particle yields can be easily checked, and thus errors and omissions in a rather complex and large particle ‘zoo’ minimized. Consider, as an example, the ratio  $\overline{\Xi^-}(\bar{d}\bar{s}\bar{s})/\Xi^-(dss)$ . Given the quark content and ignoring (at RHIC very small) isospin asymmetry, we find:

$$\frac{\overline{\Xi^-}}{\Xi^-} = \frac{\lambda_s^{-2}\lambda_q^{-1}}{\lambda_s^2\lambda_q} = \lambda_s^{-4}\lambda_q^{-2} = e^{-4\mu_s/T}e^{-2\mu_q/T} = e^{4\mu_S/T}e^{-2\mu_B/T}, \quad \mu_S = \frac{1}{2}\mu_B + \frac{T}{4}\ln\frac{\overline{\Xi^-}}{\Xi^-}. \quad (7)$$

Since all  $\Xi$  resonances which contribute to this ratio are symmetric for particles and antiparticles, and possible weak interaction feed from  $\overline{\Omega}(\bar{s}\bar{s}\bar{s})$ , and respectively  $\Omega(sss)$ , are small, these expressions are actually nearly exact. Thus we have inverted the relation

and expressed  $\mu_S$  in terms of  $\mu_B$  and the cascade ratio. This allows the reader to check for correctness results presented elsewhere. Results shown in [10] appear inconsistent by 50% while those in [12] are numerically consistent.

The important lesson to be drawn from Eq. (7) is that when we compare in a ratio particle with antiparticle we ‘see’ the chemical potentials. As we shall see below and use in section 4, the chemical non-equilibrium parameters are probed with *products* of yields of particles and antiparticles.

Near to chemical equilibrium, we use three non-equilibrium parameters,  $\gamma_s$ , and  $\gamma_u, \gamma_d$  or equivalently just two parameters introducing,  $\gamma_q = \sqrt{\gamma_u \gamma_d}$ . In quark matter, these coefficients express the approach to the expected chemical equilibrium yield by the quark abundances. In a coalescence hadronization process, gluons fragment into quark pairs and the net yields of quarks and antiquarks of all flavors is redistributed among all individual hadrons. Hence even if there were no change of the quark pair number in hadronization, the values of  $\gamma_u, \gamma_d, \gamma_s$  in hadron gas and quark matter must differ. Moreover, the phase spaces have different size, and it is impossible in the rapidly evolving fireballs to reequilibrate several quark flavors. Thus, we have to distinguish:

$$\gamma_u^{\text{QGP}}, \gamma_d^{\text{QGP}}, \gamma_s^{\text{QGP}}, \quad \text{from} \quad \gamma_u^{\text{HG}}, \gamma_d^{\text{HG}}, \gamma_s^{\text{HG}}.$$

The lesson is that in an analysis of experimental data, we explore the properties and parameters of the hadron gas phase (HG). While these may be smooth across hadronization for the chemical potentials  $\mu_i$ , we expect the phase space occupancy parameters  $\gamma_i$  to be quite different in the confined and deconfined phase. We obtain the fugacities of all hadrons in terms of six parameters, which implicitly carry the upper index ‘HG’.

It is best to see how this works looking at typical examples:

a) baryons: protons  $p(uud)$ , antiprotons  $\bar{p}(\bar{u}\bar{u}\bar{d})$ ,  $\Lambda(uds)$ ,  $\bar{\Lambda}(\bar{s}\bar{s}\bar{s})$ , etc:

$$\Upsilon_p = \gamma_u^2 \gamma_d e^{2\mu_u + \mu_d}, \quad \Upsilon_{\bar{p}} = \gamma_u^2 \gamma_d e^{-2\mu_u - \mu_d}, \quad \Upsilon_{\Lambda} = \gamma_u \gamma_d \gamma_s e^{\mu_u + \mu_d + \mu_s}, \quad \Upsilon_{\bar{\Lambda}} = \gamma_s^3 e^{-3\mu_s}. \quad (8)$$

b) mesons:  $\pi^+(u\bar{d})$ ,  $\pi^-(\bar{u}d)$ ,  $K^-(\bar{u}s)$ ,  $\phi(\bar{s}s)$ , etc:

$$\Upsilon_{\pi^+} = \gamma_u \gamma_d e^{\mu_u - \mu_d}, \quad \Upsilon_{\pi^-} = \gamma_u \gamma_d e^{-\mu_u + \mu_d}, \quad \Upsilon_{K^-} = \gamma_u \gamma_s e^{-\mu_u + \mu_s}, \quad \Upsilon_{\phi} = \gamma_s^2. \quad (9)$$

Note that in the products of particle  $\Upsilon_P$  and antiparticle  $\Upsilon_A$  fugacity the chemical potentials  $\mu_i$  always cancel  $\Upsilon_P \Upsilon_A = f(\gamma_i)$ .

In the statistical hadronization approach, we have the same value of  $\Upsilon$  for all hadrons with the same valance quark content. For example  $\Upsilon_p = \Upsilon_{\Delta^+}$ . Thus, we assume tacitly that the relative population of heavier resonances is in chemical equilibrium with the lighter states. This means that statistical hadronization resolves the valance quark and antiquark distribution and does not allow for the possibility that heavier resonances may simply not be populated. This method, thus, is most suitable for a hadronizing quark matter fireball, and may miss important features of a hadron fireball which never entered the deconfined phase.

The physical properties of the gas of hadrons with  $\gamma_u, \gamma_d, \gamma_s \neq 1$  have certain highly desirable properties. Consider the properties of the pion gas as function of  $\gamma_q$ , and in particular the entropy (B for Bosons and F for fermions):

$$S_{\text{B/F}} = \int \frac{d^3p d^3x}{(2\pi\hbar)^3} [\pm(1 \pm f) \ln(1 \pm f) - f \ln f], \quad f_\pi = \frac{1}{\gamma_q^{-2} e^{\frac{E_\pi}{T}} - 1}. \quad (10)$$

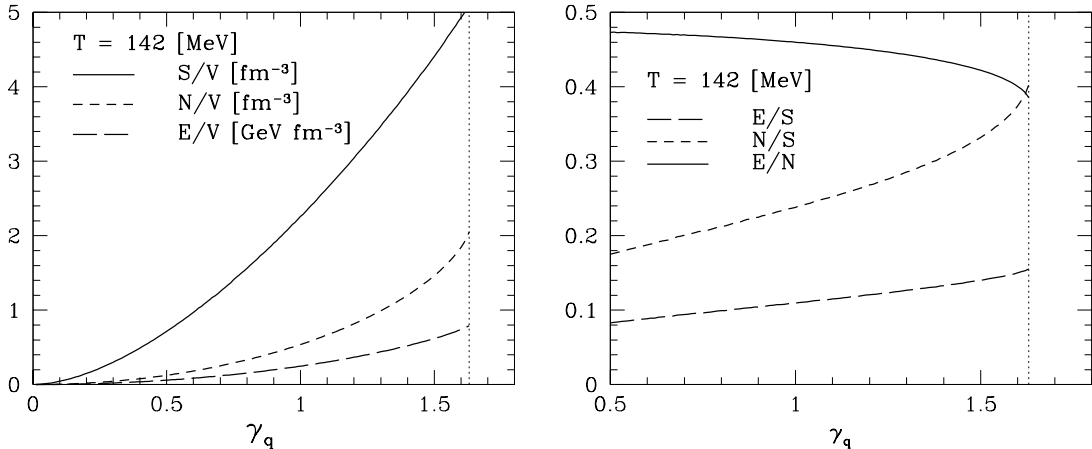


Figure 3. Pion gas properties as function of chemical nonequilibrium parameter  $\gamma_q$ .

Here,  $E_\pi = \sqrt{m_\pi^2 + p^2}$ . We see, in figure 3, that the entropy density is rising rapidly and it nearly doubles with  $\gamma_q$  increasing from the equilibrium value  $\gamma_q = 1$  toward condensation point  $\gamma_q^2 = e^{m_\pi/T}$ . This high entropy content of the oversaturated pion gas allows the sudden hadronization of QGP without reheating or inflation (volume expansion). A striking feature of the experimental data analysis which allows for  $\gamma_q$  is the maximization of entropy density in pion gas, *i.e.*, natural tendency toward the value  $\gamma_q^2 = e^{m_\pi/T}$ .

#### 4. DATA ANALYSIS

There are in our approach at most 6 chemical parameters, and hadronization temperature. Especially at RHIC, we need not distinguish the light flavors  $u, d$  and thus the number of statistical parameters is reduced by two. A further reduction is arrived at when we demand that strangeness balances anti-strangeness locally, and finally the requirement that when entropy rich quark-gluon plasma hadronizes, the yields of hadrons are maximizing the entropy content of hadrons, yields  $\gamma_q^2 = e^{m_\pi/T}$ . Thus, we are in fact needing just two chemical parameters which are usually  $\lambda_q$  and  $\gamma_s$ . Both at SPS [13] and at RHIC [14], there is good evidence for a single freeze-out to apply, in consistency with the sudden hadronization hypothesis. In other words, one single temperature allows to understand both yields and spectra of hadrons.

The computation of the particle yields is much simpler than for SPS. For central rapidity, we have, at RHIC-130, approximate longitudinal scaling. Thus, we can act as if a series of fireballs at all rapidities was present. Then, we simply evaluate the full phase-space yields in order to obtain particle ratios. We do not include in our analysis trivial results such as  $\pi^+/\pi^- = 1$ . We also do not fit the results for  $K^*$  and  $\bar{K}^*$  since the reconstructed yields depend on the degree of rescattering of resonance decay products.

We first convince ourselves that the introduction of chemical non equilibrium in the study of hadron abundances is necessary — even though one could argue that if it is not needed, the data fit will converge to chemical equilibrium condition. Therefore before we present an overall fit of many particle yields, we present a short but persuasive argument.

As noted, when we evaluate the product of particle and antiparticle yields, the chemical

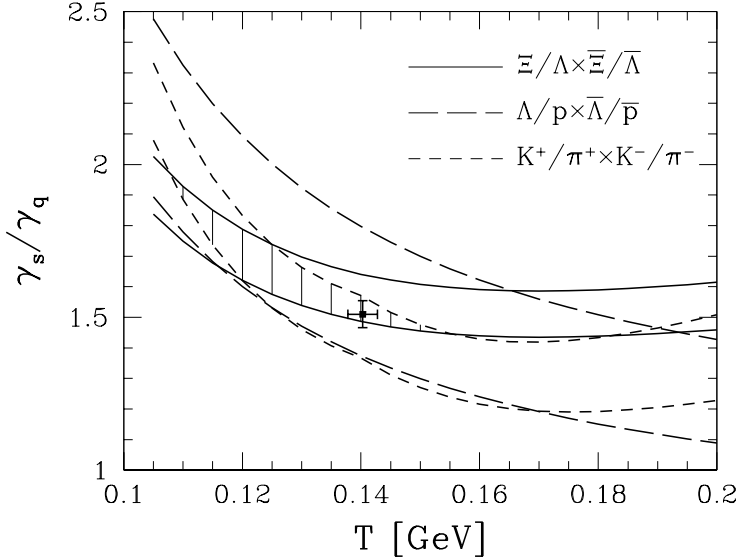


Figure 4. Ratios of products of particle and antiparticle abundances in the  $T$ - $\gamma_s/\gamma_q$  plane. Ranges derived from data shown in table 1.

potentials  $\mu_i$  cancel. Studying such products allows to focus only on  $T, \gamma_q, \gamma_s$ . We next identify three ratios involving products of particles and antiparticles:

$$\sqrt{\frac{\Xi\bar{\Xi}}{\Lambda\bar{\Lambda}}} \propto \frac{\gamma_s}{\gamma_q} e^{-\frac{m_{\Xi}-m_{\Lambda}}{T}}; \quad \sqrt{\frac{\Lambda\bar{\Lambda}}{p\bar{p}}} \propto \frac{\gamma_s}{\gamma_q} e^{-\frac{m_{\Lambda}-m_N}{T}}; \quad \sqrt{\frac{K^-K^+}{\pi^-\pi^+}} \propto \frac{\gamma_s}{\gamma_q} e^{-\frac{m_K-m_\pi}{T}}. \quad (11)$$

By comparing mesons with mesons, and baryons with baryons we reduce uncertainties about excluded volume.

The ratios considered in Eq. (11) have only two parameters  $T$  and  $\gamma_s/\gamma_q$ . Thus, it is possible to present, in a two dimensional figure, how these three ratios behave, as is seen in figure 4 for the experimental data obtained at RHIC-130 (see table 1 below). Dashed area shows the allowed parameter domain. The cross in the figure is the result of global data analysis discussed below where the ratio of baryons to mesons, not used here, fixes the temperature. While the kaon to pion ratio would tolerate within one standard deviation the chemical equilibrium, the baryon double ratios, and in particular the more strange cascades, are clearly demanding a value of  $\gamma_s/\gamma_q > 1$ .

We use the latest experimental results for the ratio of hyperons to nucleons (yields of  $p, \bar{p}$  are weak decay feed corrected,  $\Lambda, \bar{\Lambda}$  are uncorrected) [16]. This result is nearly by a factor *two* different from the experimental data stated in [12], and this reference also does not consider  $\Xi, \bar{\Xi}$  results other than their ratio, and is therefore consistent with the chemical equilibrium in the result of its analysis.

A global fit to the experimental data for RHIC-130 is given in table 1. We consider here 21 particle ratios. In some cases within the error other results from same and/or another collaboration are available, our selection is somewhat subjective, but does not influence in essential way the general conclusions which follow. In the three last columns, the results for both chemical equilibrium (last column) and non-equilibrium fits are seen.

Next to the fitted ratios, we show in parenthesis the contribution to the error ( $\chi^2$ ) for each entry. We consider statistical errors for the experimental results, since much of the

Table 1

Central-rapidity hadron ratios at RHIC- $\sqrt{s_{NN}} = 130$  GeV. From top to bottom: experimental results, fitted chemical parameters, the physical properties of final state hadron phase-space, and the fitting error. Columns: ratio considered, data value with reference, two non-equilibrium fits, and in the last column, the chemical equilibrium fit. The superscript \* indicates quantities fixed and not fitted. The superscript † indicates the error given is dominated by theoretical considerations. Subscripts  $\Xi, \Lambda$  mean that these values include weak cascading given in heading of table. In parenthesis, we show the contribution of the particular result to the total  $\chi^2$ .

			100% $\Xi \rightarrow Y$	40% $\Xi \rightarrow Y$	40% $\Xi \rightarrow Y$
	Data	Ref.	40% $Y \rightarrow N$	40% $Y \rightarrow N$	40% $Y \rightarrow N$
$\bar{p}/p$	$0.71 \pm 0.06$	[16]	0.672(0.4)	0.677(0.3)	0.688(0.1)
$\bar{\Lambda}_\Xi/\Lambda_\Xi$	$0.71 \pm 0.04$	[19]	0.750(1.0)	0.747(0.8)	0.757(1.4)
$\bar{\Xi}/\Xi$	$0.83 \pm 0.08$	[17]	0.793(0.2)	0.803(0.1)	0.818(0.0)
$K^-/K^+$	$0.87 \pm 0.07$	[18]	0.925(0.6)	0.924(0.6)	0.933(0.8)
$K^-/\pi^\pm$	$0.15 \pm 0.02^\dagger$	[18]	0.156(0.1)	0.157(0.1)	0.150(0.0)
$K^+/\pi^\pm$	$0.17 \pm 0.02^\dagger$	[18]	0.169(0.0)	0.170(0.0)	0.161(0.2)
$\bar{\Lambda}_\Xi/h^-$	$0.059 \pm 0.004^\dagger$	[19]	0.057(0.6)	0.049(6.7)	0.047(9.6)
$\bar{\Lambda}_\Xi/h^-$	$0.042 \pm 0.004^\dagger$	[19]	0.042(0.0)	0.036(2.0)	0.035(2.8)
$\Lambda_\Xi/p$	$0.90 \pm 0.12$	[16]	0.805(0.6)	0.662(3.9)	0.494(11.5)
$\bar{\Lambda}_\Xi/\bar{p}$	$0.93 \pm 0.19$	[16]	0.899(0.0)	0.731(1.1)	0.543(4.1)
$\pi^\pm/p_\Lambda$	$9.5 \pm 2$	[18]	9.4(0.0)	9.2(0.6)	7.4(27.7)
$\pi^\pm/\bar{p}_\Lambda$	$13.4 \pm 2.5$	[18]	13.7(0.1)	13.3(0.0)	10.6(9.6)
$\Xi^-/\pi$	$0.0088 \pm 0.0008^\dagger$	[17]	0.0092(0.2)	0.0097(1.2)	0.0069(5.8)
$\Xi^-/h^-$	$0.0085 \pm 0.0015$	[17]	0.0076(0.3)	0.0079(0.2)	0.0056(3.8)
$\Xi^-/h^-$	$0.0070 \pm 0.001$	[17]	0.0061(0.9)	0.0064(0.4)	0.0046(6.0)
$\Xi^-/\Lambda$	$0.193 \pm 0.009$	[17]	0.190(0.1)	0.189(0.2)	0.132(45.4)
$\Xi^-/\bar{\Lambda}$	$0.221 \pm 0.011$	[17]	0.207(1.6)	0.206(1.9)	0.144(48.4)
$\Omega/\Xi^-$			0.20	0.21	0.18
$\bar{\Omega}/\Xi^-$			0.22	0.23	0.20
$\Omega/h^-$	$0.0012 \pm 0.0005$	[20]	0.0015(0.4)	0.0016(0.7)	0.0010(0.13)
$\bar{\Omega}/\Omega$	$0.95 \pm 0.1$	[20]	0.87(0.7)	0.88(0.5)	0.90(0.3)
$\phi/K^-$	$0.15 \pm 0.03$	[21]	0.174(0.6)	0.177(0.9)	0.148(0.0)
$\phi/h^-$	$0.021 \pm 0.001$	[21]	0.022(1.3)	0.023(2.5)	0.018(10.2)
$T$			$140.3 \pm 1.1$	$142.5 \pm 1.2$	$165.8 \pm 2.2$
$\gamma_q^{\text{HG}}$			1.64*	1.63*	1*
$\lambda_q$			$1.0700 \pm 0.0076$	$1.0686 \pm 0.0076$	$1.0654 \pm 0.0082$
$\mu_B$ [MeV]			28.5	28.4	31.3
$\gamma_s^{\text{HG}}/\gamma_q^{\text{HG}}$			$1.50 \pm 0.04$	$1.48 \pm 0.04$	1*
$\lambda_s$			1.0243*	1.0218*	1.0186*
$\mu_S$ [MeV]			6.1	6.4	7.4
$E/b$ [GeV]			34.7	34.3	34.1
$s/b$			9.5	9.3	7.0
$S/b$			233.4	227.7	238.5
$E/S$ [MeV]			148.7	150.5	143.0
$\chi^2/\text{dof}$			$10/(21-3)$	$25/(21-3)$	$188/(21-2)$
				J.R./J.L.	26.10.2002

systematic error should cancel in the particle ratios. However, we do not allow, when pion multiplicity is considered, for errors smaller than  $\simeq 10\%$ , which is our estimated error in the theoretical evaluation of the pion yield due to incomplete understanding of the high mass hadron resonances. Some of the experimental results are thus shown with a ‘theoretical’ error. When such an enlargement of the experimental error is introduced, a dagger as superscript appears in the experimental data second column in table 1.

The high yields of hyperons require significant (30-40%) yield corrections for unresolved weak decays. Some experimental results are already corrected in this fashion: the weak cascading corrections were applied to the most recent  $p$  and  $\bar{p}$  results by the PHENIX collaboration [16], and in the  $\Xi/\Lambda$  and  $\bar{\Xi}/\bar{\Lambda}$  ratio of the STAR collaboration we use here [17]. However, some of the results we consider are not yet corrected [18,19], and are indicated in the first column in table 1 by a subscript  $\Lambda$  or  $\Xi$ . We present two non-equilibrium fits, left with 100%  $\Xi \rightarrow Y$  cascading acceptance and with 40%  $Y \rightarrow N$  acceptance. Then, a non-equilibrium fit with 40%  $\Xi \rightarrow Y$  and 40%  $Y \rightarrow N$ , and in the last column, the chemical equilibrium fit with 40% cascading.

Below the fit results, we show the statistical parameters which are related to each fit, and at the very bottom the  $\chi^2$  of the fit. We observe a considerable improvement in the statistical significance of the results of chemical non-equilibrium fits. The results, shown in the table 1, are obtained minimizing in the space of 3 parameters: the chemical freeze-out temperature  $T$ , and 2 chemical parameters  $\lambda_q, \gamma_s$ , the value of  $\gamma_q$  is set at its maximal value,  $\gamma_q^2 = e^{m\pi/T}$ , and the value of  $\lambda_s$  is derived from the strangeness conservation constraint. Freeing these parameters does not alter the results, the fit converges to local strangeness neutrality, within a few percent, and to full pion phase space saturation.

We note that several particle yields are not properly described in the last column of table 1, and hence a large  $\chi^2$  results in this chemical equilibrium fit. However, on a logarithmic scale only results involving  $\Lambda, \bar{\Lambda}$  would be clearly visible as a discrepancy. The second and third last column show result of chemical non-equilibrium fits bracketing the  $\Xi$ -cascading, and yielding an excellent confidence level.

In the bottom of table 1, we see that the chemical non-equilibrium fit specific strangeness content  $s/b \simeq 9.5$  is nearly 40% greater than the chemical equilibrium result. This originates in  $\gamma_s/\gamma_q \simeq 1.5$  (*i.e.*,  $\gamma_s \simeq 2.5$ ). This specific yield of strangeness and strangeness occupancy we measure in the phase space after hadronization is consistent with the expected QGP properties before hadronization with nearly saturated strangeness phase space. The Wróblewski ratio [22],  $W = 2\langle s\bar{s} \rangle / (\langle u\bar{u} \rangle + \langle d\bar{d} \rangle)$ , is nearly proportional to  $\gamma_s/\gamma_q$  and it increases by 40% at RHIC-130 compared to SPS. However, an analysis with  $\gamma_s/\gamma_q \simeq 1$  will not report this enhancement [23].

Our chemical nonequilibrium results yield a low freeze out temperature  $T_h = 140-142$  MeV. This is considerably less than the temperature of phase transformation,  $T_H$  which might have been naively expected. This range of hadronization temperature now seen agrees better with the expectations we had upon consideration of the effect of the fast expansion of QGP [24]. We believe that the wind of expending quarks and gluons adds to the thermal pressure and the combined kinetic and thermal pressure of exploding quark-gluon plasma can press out the confining vacuum even at lower temperature [25].

The results we find strongly favor chemical non-equilibrium description of the hadronization process. A non-equilibrium chemical analysis of heavy-ion particle yields offers pro-

found insight into the physical properties of the dense hadronic matter formed in the relativistic heavy-ion collisions and allows to infer conditions prevailing in the deconfined phase. While the equilibrium Fermi model provides a first impression about the range of freeze-out temperatures, our post-Fermi model resolves the ‘fine structure’ of the hadronization yields.

## REFERENCES

1. E. Fermi, *Prog. Theor. Phys.* **5** (1950) 570.
2. I. Pomeranchuk, *Proc. USSR Academy of Sciences (in Russian)* **43** (1951) 889.
3. R. Hagedorn, *Suppl. Nuovo Cimento* **2** (1965) 147.
4. R. Hagedorn, *Nuovo Cimento A* **56** (1968) 1027.
5. R. Hagedorn and J. Rafelski , *Phys. Lett. B* **97**, (1980) 136; and “From hadron gas to quark matter I” in *Statistical Mechanics of Quarks and Hadrons*, ed. H. Satz, North Holland (1981) p. 237.
6. R. Fiore, R. Hagedorn, and F. D’Isep, *Nuovo Cimento A* **88**, 301 (1985).
7. *Hadrons and Quark-Gluon Plasma*, J. Letessier and J. Rafelski, CUP, Cambridge (2002) section 12.
8. W. Broniowski and W. Florkowski, *Phys. Lett. B* **490** (2000) 223.
9. R. Hagedorn, *Nuovo Cimento* **52**, (1967) 1336.
10. P. Braun-Munzinger, D. Magestro, K. Redlich and J. Stachel, *Phys. Lett. B* **41**, (2001) 518.
11. F. Karsch, *Nucl. Phys. A* **698**, (2002) 199; *Springer Lect. Notes Phys.* **583**, (2002) 209.
12. W. Broniowski and W. Florkowski, “Thermal approach to RHIC” hep-ph/0209286 .
13. G. Torrieri and J. Rafelski, *New J. Phys.*, **3** (2001) 12.
14. W. Broniowski and W. Florkowski. *Phys. Rev. Lett.*, **87** (2001) 27-2302.
15. J. Letessier and J. Rafelski, *Int. J. Mod. Phys., E* **9**, (2000) 107.
16. C. Adcox, *et al.*, PHENIX collaboration, *Phys. Rev. Lett.* **89**, (2002) 09-2302.
17. J. Castillo, *et al.*, STAR collaboration, July 2002 Presentations at Nantes, Quark matter 2002, this volume; and Ph.D. Thesis, University Nantes, 2002.
18. C. Adcox *et al.*, PHENIX collaboration. *Phys. Rev. Lett.* **88** (2002) 24-2301.
19. C. Adler *et al.*, STAR collaboration. *Phys. Rev. Lett.* **89**, (2002) 09-2301.
20. C. Suir, *et al.*, STAR Collaboration, July 2002 Presentations at Nantes, Quark matter 2002, this volume.
21. C. Adler *et al.*, STAR collaboration. *Phys. Rev. C* **65**, (2002) 04-1901; and July 2002 Presentations at Nantes, Quark matter 2002, by STAR collaboration in this volume.
22. A. Wróblewski, *Acta Phys. Pol. B* **16**, (1985) 379.
23. F. Becattini, *J. Phys. G* **28**, (2002) 1553.
24. J. Rafelski and J. Letessier. *Phys. Rev. Lett.*, **85** (2000) 4695.
25. T. Csorgo, and J. Zimanyi, “Inflation of fireballs, the gluon wind and the homogeneity of the HBT radii at RHIC”, *nucl-th/0206051* .